Preprint Title	Spherical Gold Nanoparticles (AuNPs) Formation by Selected Intracellular Protein Fraction of Fungi
Authors	Huangrui Liu, Nengwu Zhu, Deliang Luo, Minting Li, Pingxiao Wu and Yaojun Mo
Article Type	Full Research Paper
Supporting Information File 1	Additional experimental details.docx; 6.7 MB
ORCID® iDs	Nengwu Zhu - https://orcid.org/0000-0002-5414-884X

Spherical gold nanoparticles (AuNPs) formation by selected intracellular protein fraction of *fungi*

Huangrui Liu[1], Nengwu Zhu [1,2,3,4*], Deliang Luo[1], Minting Li[1], Pingxiao Wu [1,2,3,4], Yaojun Mo[1]

[1] School of Environment and Energy, South China University of Technology, Guangzhou 510006, P.R. China

[2] The Key Lab of Pollution Control and Ecosystem Restoration in Industry Clusters, Ministry of Education, Guangzhou 510006, P.R. China

[3] Guangdong Environmental Protection Key Laboratory of Solid Waste Treatment and Recycling, Guangzhou 510006, P.R. China

[4] Guangdong Engineering and Technology Research Center for Environmental Nanomaterials, Guangzhou 510006, China

[*]Corresponding author.

Tel./fax: +86-20-3938 0522.

E-mail address: nwzhu@scut.edu.cn

Abstract

Pycnoporus sanguineus and its intracellular protein extracts (IPE) were proved to be efficient to produce gold nanoparticles (AuNPs) with uncontrollable morphologies and sizes. In order to improve the quality of the AuNPs, the IPE of *P. sanguineus* were successfully graded into five fractions by ultrafiltration approach, reacting with $AuCl_4^-$ respectively. Comparing with the original IPE and other fractions, proteins of molecular weight around 10–30 kDa obtained AuNPs with the most concentrated size smaller than 30 nm in high yield (above 90%) and the most homogeneous shape (87% spherical shapes). Under the optimized conditions of 25 ml 10–30 kDa dosage, pH=4, 30 ℃ and 0.5 mM $AuCl_4^-$, the proportion of spherical AuNPs with narrower size (6–25 nm) rose up to 93.5%. The mechanism might be mainly contributed by the absorption of substrate by the abundant of amine and carboxyl functional groups, the reduction and formation of AuNPs with smaller size by larger proportion of lysine and tyrosine, and the generation of spherical products with low content of amino acids for anisotropic growth. This work provided evidence of efficient utilization of microbes in biosynthesis of precious metal nanoparticles and potential enhancement of the performance of biosynthesized products.

Keywords

biosynthesis; gold nanoparticles; intracellular protein extract; protein ultrafiltration; *Pycnoporus sanguineus*

Introduction

Gold nanoparticles (AuNPs) are the tiny particles of gold with a diameter of 1–100 nm. It possesses distinct physicochemical properties such as high electron density, dielectric properties, and good biocompatibility, gaining interest in technological applications such as sensors [1, 2], electronic devices [3], bioimaging [4, 5], and catalysis [6, 7]. It is well known that the size and shape of AuNPs play a vital role in their performance and application, giving those remarkable electrical and optical properties and meeting the application of practical technology. Thus, it is meaningful to study the controllable synthesis system of AuNPs.

Various chemical and physical synthesis methods successfully produce pure and well-defined nanoparticles [8]. For example, Kariuki et al. [9] using pyromellitic dianhydride-p-phenylene diamine – PPDDs to synthesize multibranched, monodispersed gold nanoflowers at room temperature, which exhibited different degrees of anisotropy and protuberance lengths after changing the ratio of PPDDs and $HAuCl_4 \cdot 3H_2O$. In additions, Biological synthetic routes are the hotspots in the field of synthesizing AuNPs because of many merits including non-toxic, eco-friendly, and time-saving, receiving increasing attention [10]. Several microorganisms such as fungus, algae, bacteria, yeasts, actinomycetes, and plants and their biological extract have been investigated [11]. Faramarzi et al. [12] successfully synthesized AuNPs in the range of 71–266 nm by the purified laccase from *Paraconiothyrium variabile*. Besides, previous study of our team [13] reported on preparation of AuNPs by using intracellular protein extracts (IPE) of a white rot fungal strain *Pycnoporus sanguineus*, which could produce large quantities of reductases such as laccases that can be handled easily during biosynthesis. The biosynthesized products did well in the degradation of 4-nitroaniline but existed large developmental space on shape and size control. Although biological approach still has immeasurable prospect, the

knowledge of formation mechanisms and the controllability of the nanoparticles is still scarce.

In recent years, many studies were proposed to use inactive cell biomass, proteins/enzymes, chitosan or other biological extracts followed by the control of related critical parameters to synthesize shape-controlled AuNPs [10]. Shen et al. [14] used three microbial cell-free extracts to compare the characteristics of AuNPs and demonstrated that cell-free extracts of fungi formed more uniform and monodisperse size of AuNPs with average sizes at 9.5 nm. Italiano et al. [15] reported that the biosynthesized AuNPs were spherical in shape with an average size of 10 ± 3 nm by using the metabolically quiescent biomass of photosynthetic bacterium *Rhodobacter sphaeroides*. Interestingly, Xie et al. [16] separated the *Chlorella vulgaris* extract into 8 fractions to obtain AuNPs, showing that the protein with a molecular weight of 28 kDa produced gold nanoplates with distinctive triangular and hexagonal shapes in high yields (approximately 90 %). The studies mentioned above provide clues to enhance the applicability of *P. sanguineus* in AuNPs synthesis and increase proportion of monodisperse AuNPs through separating IPE to different fraction, facilitating the efficient use in the future. But it is rarely reported.

Herein, we proposed a novel method to obtain outstanding AuNPs products with higher yield and monodisperse size by specific fraction of IPE. The underlying mechanism of the synthesis of nanoparticles by the specific fraction of IPE was studied through FTIR, XPS and Amino acid analysis.

Results and Discussion

Comparison of AuNPs' formation by different fractions of IPE

The presence of proteins in IPE was confirmed by SDS-PAGE analysis (Supporting Information File 1, Figure S1, lane 1). It shows that three protein bands with molecule weight of 10–30, 30–50 and 50–100 kDa were intense and other were fainter. Also, the obtained five fractions of IPE (P1–P5) by ultrafiltration approach were confirmed by SDS-PAGE analysis (Supporting Information File 1, Figure S1, lane 2–6). It appears that bands 3–5 were intense and lane 2 and lane 6 were not obvious because of low protein content.

The ability of IPE and five different fractions of IPE for AuNPs synthesis were investigated by UV-vis absorption intensity and gold recovery rate (Figure 1). When reacting with $HAuCl_4$, the color of the mixture was changed from yellow to purple and different fractions showed different color shades after 24 h reaction. UV-vis spectrum pattern from all the six biomaterials were similar (Figure 1A). The UV-vis spectrum showed a peak around 520–550 nm, indicating the formation of AuNPs because of the surface plasmon resonance (SPR) of AuNPs [17]. A sharp SPR was observed for IPE and the others were weak to some extent. It could be said that IPE separating weakened the ability of reducing $AuCl_4^-$. Absorption peak of the UV-vis spectrum obtained from P2 was also high compared with their counterparts, which confirmed the higher productivity of AuNPs. In additions, the AuNPs prepared by P2 was found to be blue shifted, in comparison with that prepared by IPE. Rogers et al. [18] reported a strong correlation between the particle size and the maximum absorption peak and they found that as the particle size increased, the maximum absorption were found to be red shifted. The similar regulations appeared in recovery analysis. Figure 1B depicted that IPE had the highest gold recovery rate (95.58%), the recovery rate of P2 also reached 90.33%, ranking first among the other four fractions of IPE. Based on univariate analysis results of the gold recovery, P2 had significant difference with other fraction of IPE on the yield of AuNPs (P<0.05) while IPE and

P1–P5 had extremely significant effect (*P*=0.001). It demonstrates that P2 performed well in UV-vis intensity and gold recovery.

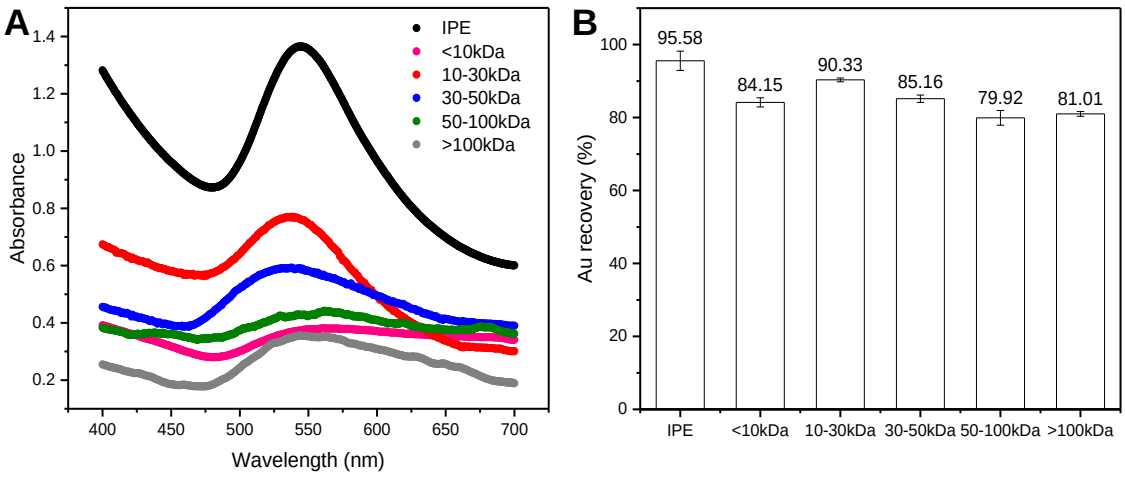

Figure 1: UV-vis spectra (A) and recovery (B) of AuNPs obtained using IPE and fractions P1–P5.

The analysis of size and morphology of AuNPs further validated the results above by typical TEM micrographs (Supporting Information File 1, Figure S2–S4 and Figure 2). Although IPE has the highest gold recovery rate, it failed to do well in the control of morphology and size. The AuNPs appeared to be in various shape in Figure 2A, which were obtained by IPE. The nanoparticles, which were 8–122 nm in size along their height (Figure 2B), were spherical, triangular, truncated triangular, hexagonal, trapezoid and the other irregular shape in geometry. By comparing IPE and its other fractions, P2 preferred synthesizing spherical AuNPs and smaller particle sizes of AuNPs (Figures 2C and 2D). It is found that the calculated sizes of AuNPs from P2 ranged between 8 and 30 nm and the proportion of 10–20 nm nanoparticles was up to 75.4%. Besides, P2 had the advantage on shape control, the proportion of synthesizing spherical AuNPs was 87%, higher than the other five groups (Table 1).

The studies have confirmed that the physiochemical properties of the composites are influenced greatly by the nanostructure and size of nanoparticles, the monodisperse nanoparticles can absorb more interest in technological application in genetic, targeting, optical, medical and electronic fields and so on [3, 19].

Moreover, P1, P3 to P5 appeared to lack sufficient ability to synthesize more uniform and monodisperse size of AuNPs. The particle sizes produced by P1 varied from 7 nm to 185 nm and the yield of small size (<30 nm) was 58.1%. Besides, the particle shapes were concentrated on spherical (73%), and the rod-like AuNPs also accounted for a certain proportion (5%) (Supporting Information File 1, Figure S2). Figure 2F showed that P3 only produced AuNPs whose sizes smaller than 42 nm but the gold recovery of P3 was low. When it came to P4 (Supporting Information File 1, Figure S3), it is noteworthy that the sizes distribution of AuNPs was narrow (85.4%, AuNPs is range 10–20 nm), but slight agglomeration behavior appeared because of synthesizing more than 90% irregularly shaped particles and smaller sizes which resulted in larger surface area [20]. Furthermore, the particle sizes produced by P5 ranged from 5 to 91 nm and AuNPs were various in shape (Supporting Information File 1, Figure S4). TEM characterizations and the recovery of AuNPs showed that fraction P2 had superiority on size, morphology control and synthesizing in high yield (>90%). Thus, P2 was the optimum fraction of IPE.

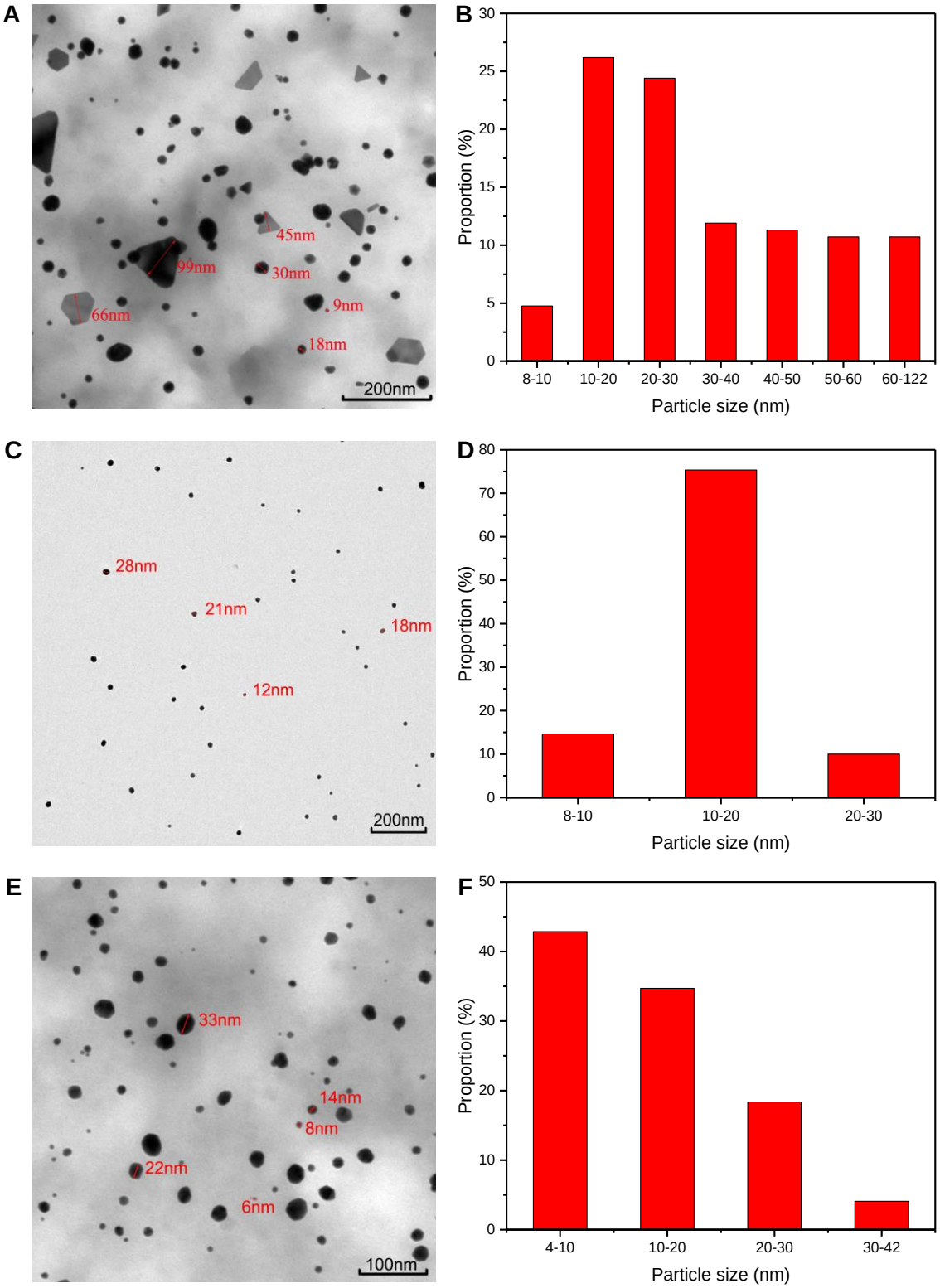

Figure 2: TEM micrograph of AuNPs produced by IPE (A), P2 (C), P3 (E), and corresponding diagram of the nanoparticle size distribution (B, D and F).

Table 1: Summary of the proportion of spherical AuNPs from IPE and fractions P1-P5.

Fraction	IPE	P1	P2	P3	P4	P5
The proportion of spherical AuNPs	65%	73%	87%	74%	-	85%

Optimization of AuNPs synthesis by P2

P2 dosage, gold ion concentration and pH were involved in the study of optimum reaction conditions on the P2 fraction. As shown in Figure 3A and 3B, the absorption steadily raised in intensity as volume of P2 dosage increased with the rise of recovery from 70.98 to 94.64%. The increase in P2 dosage represented more reductive substances, which led to the enhancement of absorption peak and reduction rates. Figure 3C and 3D give information about the effect of $HAuCl_4$ concentration on gold recovery. The UV absorption intensity was highest when the concentration of $HAuCl_4$ was 0.5 mM. The other reaction systems obtained lower absorption peak because of its lower concentration of $HAuCl_4$ with fewer products or higher substrate concentration with insufficient reductants [21]. From the perspective of recovery rate, although the recovery of 0.5 M was lower than that of 0.1 M and 0.3 M, it was higher than both in terms of substrate concentration and yield. Under the system above, 0.5 M of $HAuCl_4$ was the best choice and it would be no waste due to the insufficient effective content of P2.

The synthesis of AuNPs at various pH were also studied. With the increase of pH, the absorption peak and gold recovery enhanced first and then decreased (Figure 3E and 3F). It is clearly indicated that the best formation of AuNPs was at pH 4 with the recovery of 93.49% and it was the same as the IPE reaction environment [13]. The adsorbing and reducing progress in the reaction of $HAuCl_4$ and P2 were

simultaneous [16]. When pH was low, $HAuCl_4$ existed mainly in the form of $AuCl_4^-$, it would be capped (electrostatic interaction) and reduced by $-NH_3^+$ due to the protonation of $-NH_2$ groups. However, at pH 2, the competition between the counter anions (chloride ions) of the acid and $AuCl_4^-$ strongly reduced the capability of capping and reducing [22]. Besides, the extreme pH not only effected the recovery of gold, but also led to the AuNPs growing in the unstable environment, leading to the agglomeration of the metal with dendrite/fractal structures (Supporting Information File 1, Figure S5) [23]. Along with the increase of pH value, electrostatic repulsion occurred between the protein amino acid functional groups such as carboxyl, hydroxyl functional groups with negative charge and $AuCl_4^-$. Hence, the recovery of gold from P2 declined and the intensity of absorption weakened. Thus, a crucial role played by pH in controling the shape and recovery of AuNPs synthesis was evident from the results above. Similar results could be found on the reports by Das et al. [21], Choudhary et al. [24] and Zhu et al. [22].

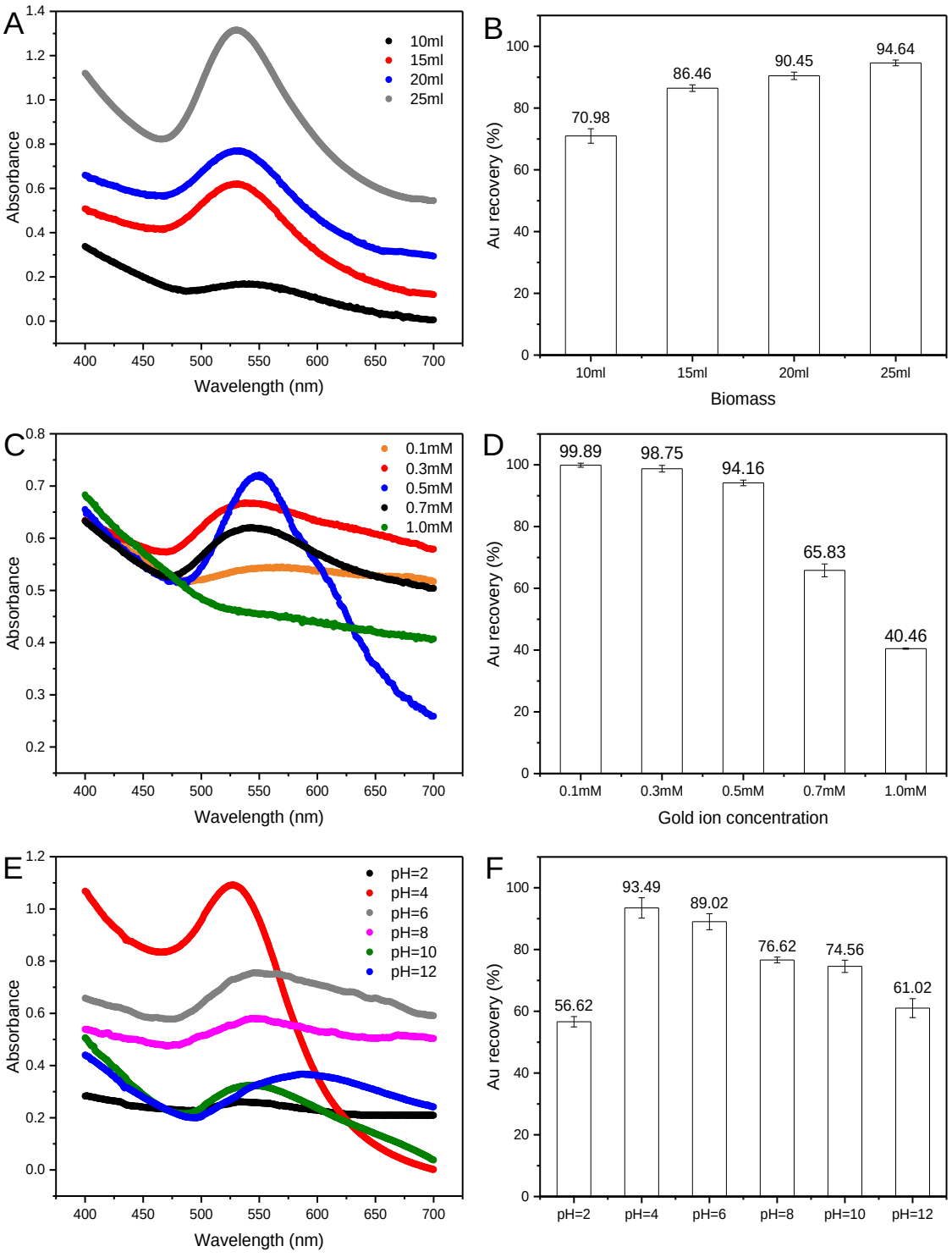

Figure 3: UV-vis spectra and bar graph of AuNPs recovery recorded from P2 with different conditions. (A and B) Effect of P2 dosage; (C and D) Effect of gold ion concentration; (E and F) Effect of solution pH.

Under the optimized conditions of 25 ml P2 dosage (protein concentration of 0.87 mg/ml), pH=4, 30 ℃ and 0.5 mM $AuCl_4^-$, the recovery of AuNPs by 10–30 kDa fraction rose to 94.64%, Size range of them changed from 8–30 nm to 6–25 nm, and the morphology of nanoscale particles was well controlled (changed from 87% to 93.5%, spherical shapes) (Figure 4). Shape and size control of AuNPs are useful in a wide range of applications, likes gold nanoclusters (smaller than 2 nm) can be used as fluorescent probes [2] and networked gold nanowires showed higher activity of catalytic properties [25]. Our study successfully obtained 10–30 kDa fraction of IPE from *P. sanguineus*, more monodisperse AuNPs were synthesized and 93.5% of AuNPs were spherical shapes, which provided the basis for improving the performance of AuNPs.

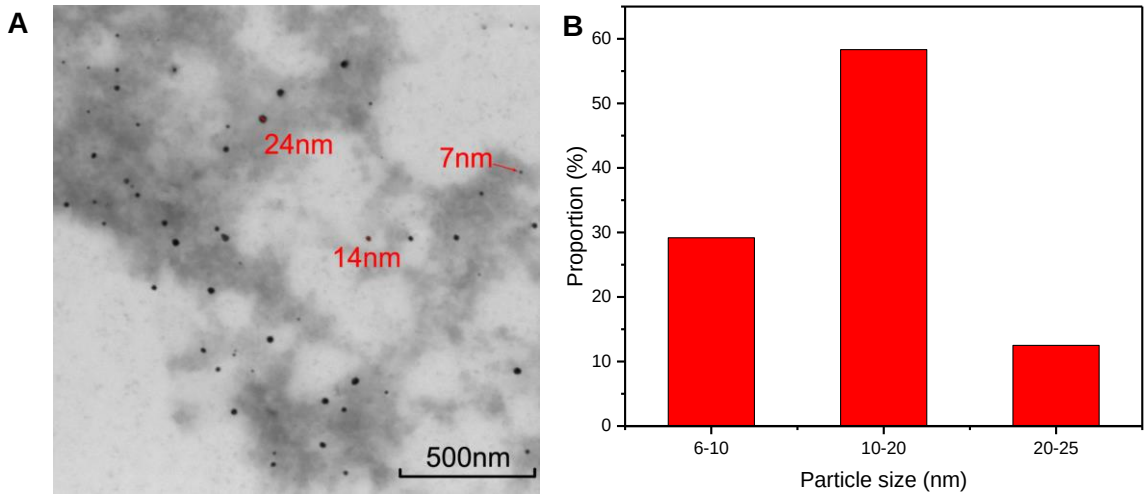

Figure 4: TEM micrograph of AuNPs produced by P2 (A) and corresponding diagram of the nanoparticle size distribution (B). Conditions: 25 ml P2 dosage (protein concentration of 0.87 mg/ml), 0.5 mM, pH=4 and 30 ℃.

The characterization of AuNPs

AuNPs produced by 10–30 kDa fraction of proteins at 25 ml P2 dosage (protein concentration of 0.87 mg/ml), 0.5 mM $AuCl_4^-$ and pH 4 were characterized FTIR, XRD. In the processes of reaction, the solution gradually changed from light yellow to light green, then deep ink green, and finally stabilized in deep purple, attributing to the difference in size and morphology formed [11]. The crystalline nature of AuNPs was investigated by the XRD analysis (Figure 5A), showing the diffraction peaks at 38.1°,44.3°,64.5°,77.5°, and 81.6°, and corresponding to the (111), (200), (220), (311) and (222) facets of the face centered cubic crystal structure, respectively. No spurious diffractions due to crystallographic impurities were found. In addition, the intensity of the (111) diffraction is much stronger than the other planes so that the (111) plane was the predominant orientation [26]. According to Scheller's formula (1), the average size of AuNPs under optimized conditions was 16.76 nm, which was consistent with the AuNPs size distribution above (Figure 4B).

$$D=0.89\lambda/(\beta\cos\varphi) \quad (1)$$

where D is the crystal diameter perpendicular to the crystal plane, λ is the emission wavelength of the copper target, the value is 0.15418 nm, β is the half-peak width of the diffraction peak, φ is the diffraction angle.

Fourier transform infrared spectroscopy (FTIR) was carried out to identify functional groups of the formation of AuNPs (Figure 5B). Before reaction, it is noticed that FTIR showed peaks at 1635 and 1403 cm^{-1} with protein characteristics, assigned to the amide I and II bands of proteins respectively [27]. The FTIR spectra changed greatly after reacting with $HAuCl_4$. Amide I band moved from 1635 cm^{-1} to 1628 cm^{-1} because of the in-plane deformed vibration by $–NH_2$. The peak at 1455 cm^{-1} disappeared whereas the peak of 1531 cm^{-1} appeared which represented stretching vibration of N-H from secondary amide II. It is demonstrated that the peak at 1408 cm^{-1} representing –COOH symmetrically stretching modes of amino acid carboxyl

groups became stronger and the strong peak of secondary amide III band at 3175 cm^{-1} appeared [28]. It is well known that free amine groups or cysteine residues in the proteins had strong capability to reduce and stabilize AuNPs [29]. The results clearly indicated that carbonyl, hydroxyl, amine, and carboxyl of proteins could participate in the reduction and subsequent stabilization of AuNPs, which were consistent with previous reports [28, 30].

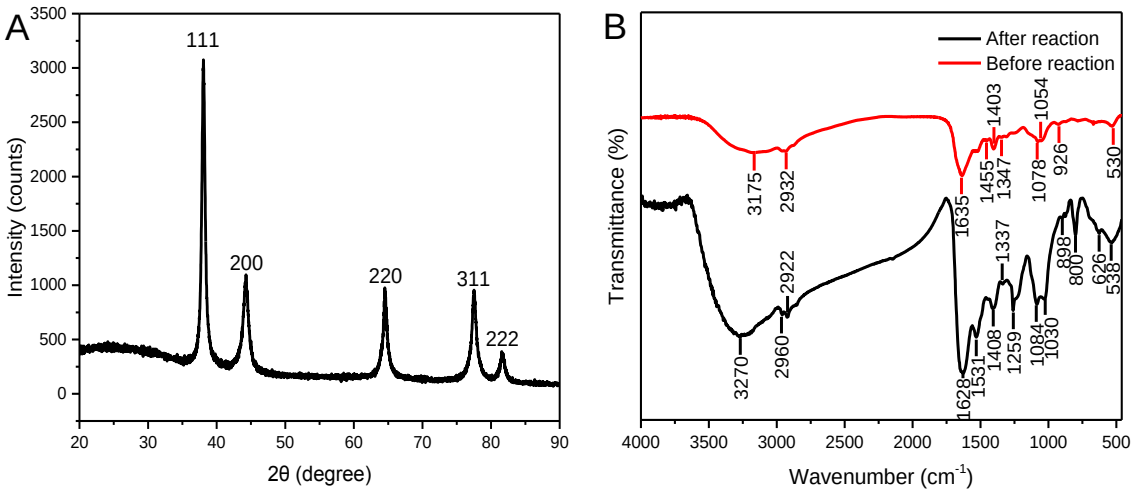

Figure 5: Representative XRD pattern of biosynthesized AuNPs (A) and FTIR spectra of the original 10–30 kDa and AuNPs (B). Conditions: 25 ml P2 dosage (protein concentration of 0.87 mg/ml), 0.5 mM, pH=4 and 30 ℃.

The speciation of Au in the reducing process were further studied through XPS. Panels A, B, C and D of Figure 6 showed the Au_{4f}, C_{1s}, N_{1s}, O_{1s} core level spectra of P2-capped AuNPs (Supporting Information File 1, Figure S6), demonstrating that different functional groups like carboxyl, amine etc. provided Au (III) binding sites for biosynthesis of Au. Figure 6A showed that Au_{4f} spectra could be deconvoluted into two distinct components centered at binding energies (BEs) of 87.29 eV and 83.62

eV, which could be assigned to Au (0) and Au (I) respectively. The small amount of Au (I) (5%) presenting on the surface of the AuNPs helped to stabilize the particles electrostatically against aggregation in solution, also indicating the formation of AuNPs through intermediate Au (I) species [2]. The C_{1s} core level centered at 284.6 eV, 286.5 eV and 288.9 eV corresponded to C-C bond, C-N bond, and the carbonyl bond respectively and the peak at 285.4 eV was caused by an indefinite carbon atom (Figure 6B). Besides, the N_{1s} core level spectrum owned three chemically distinct components, centered at the BE values of 399.6 eV, 398.3 eV and 398.9 eV (Figure 6C), which could be assigned to amide (399.6 eV) and amine groups (398.3 eV and 398.9 eV) of P2-AuNPs [23]. Figure 6D depicted three chemically distinct component of the O_{1S} core level spectrum, which referred to Carboxylic acid and amides (N-C=O, C-OH and O=C-O) [31]. All in all, the results above could be used as indirect evidences to infer the presence of proteins on the gold surface, and FTIR and XPS revealed that carbonyl, hydroxyl, amine, and carboxyl might be the major functional groups involved in the recovery and stabilization processes.

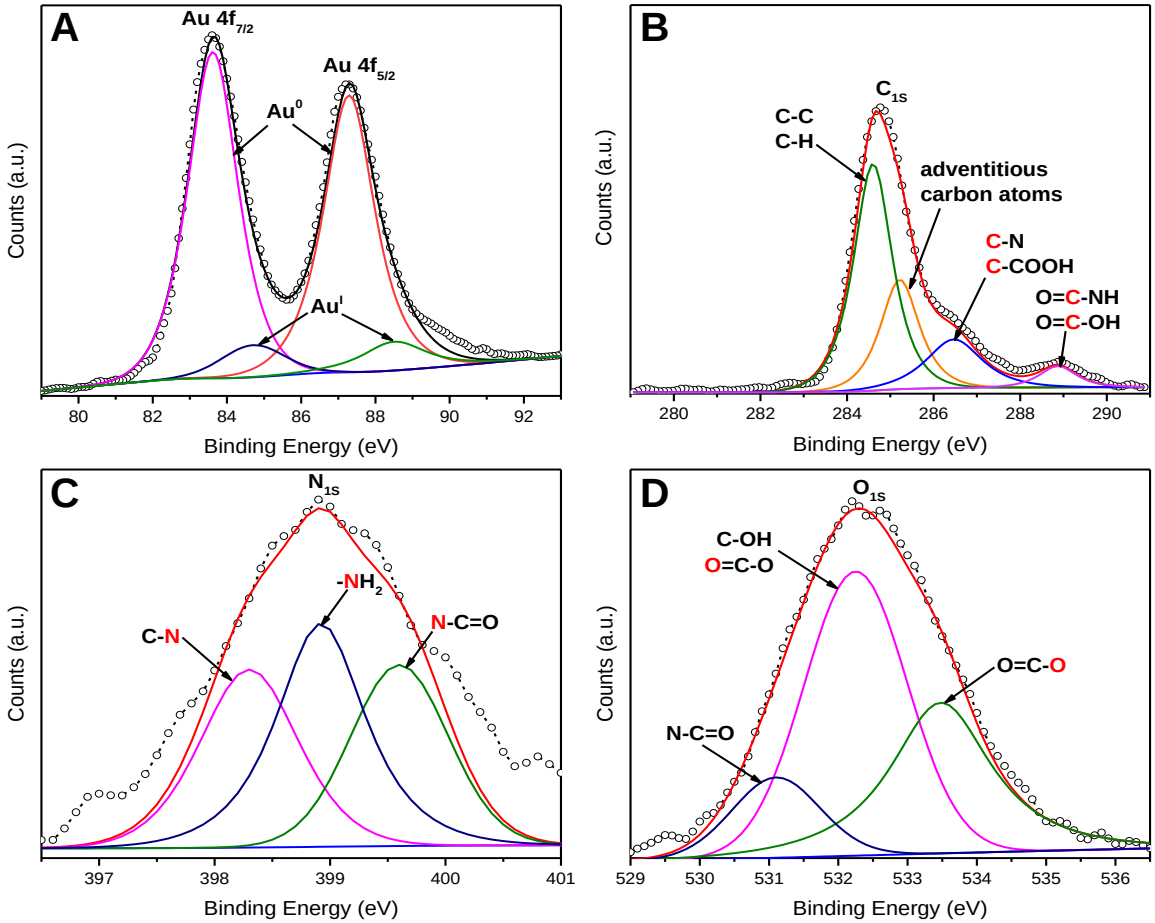

Figure 6: (A, B, C and D) Au4f, C1s, N1s and O1s core level spectra of P2-capped gold nanoparticles, respectively.

Amino acid analysis

The reduction and growth of metal nanoparticles were related to the type and proportion of amino acids in peptide chains. So amino acids of IPE and 10–30 kDa were analyzed to compare the difference at amino acid level. Glutamic acid (22.6%) and lysine (41.53%) were the main amino acids of IPE and 10–30 kDa fraction, respectively. In addition to IPE containing 10.26% lysine, the proportion of other amino acids was less than 10% (Figure 7). A significant test for ratio of the same amino acid between IPE and 10–30 kDa (Supporting Information File 1, Table S1)

found that there was no significant difference in the proportion of two samples on glycine, valine, serine and methionine (P>0.05), and other amino acids were significant different (P<0.05 or P<0.01).

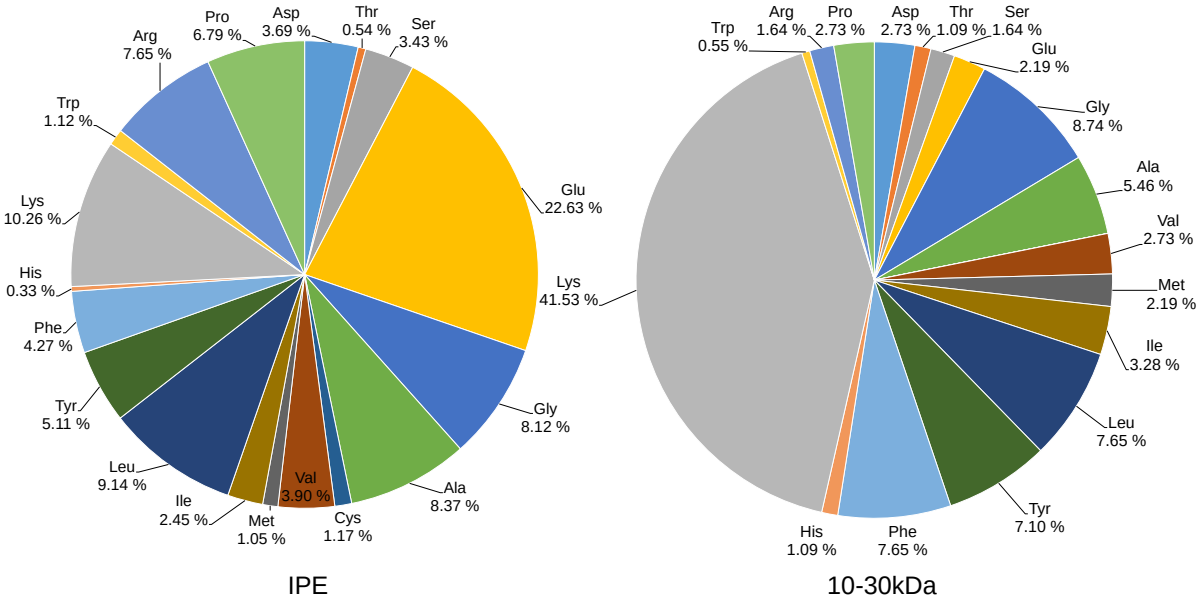

Figure 7: Amino acid composition and proportion of IPE (left) and 10–30 kDa (right).

As the largest proportion of the amino acids, lysine attracted the negative form of $AuCl_4^-$ by electrostatic action with positive charge in aqueous solution. At the same time, it acted as a reducing agent to provide ð electrons, quickly driving reduction to Au nuclei, whereas glutamic acid with negative charge in IPE was not conducive to the attraction of $AuCl_4^-$. Tan et al. [32] demonstrated that the decrease in the size of AuNPs was accompanied by the increase of reduction rate. Generally, the morphosynthesis of AuNPs was a kinetic control process, and a slow growth environment was beneficial to the selective adsorption on gold nuclei and the development of anisotropy by the capping molecules [33]. Phenyl groups and amino and hydroxyl substituents contained many mobile ð electrons, electron transfer occurred readily as the oxidized form might be energetically favored [34]. Unfortunately, IPE and 10–30 kDa fraction only contained 1.12% and 0.55% of tryptophan, respectively, which showed high affinity and reducibility for AuNPs,

contributing to the fast growth of AuNPs. Tyrosine was the second most effective amino acid at producing AuNPs, which rank NO.5 (7.1%) in 10–30 kDa, whereas IPE contained only 5.11%. Therefore, comparing with IPE, 10–30 kDa was more likely to attract $AuCl_4^-$ and had larger proportion of amino acids with higher reducibility, it was easier to generate smaller nanoparticles.

Proteins and peptides added to AuNPs synthesis solution mediate AuNPs growth via direct binding to the metallic surface [35]. Imidazole, hydroxyl, amide, and carboxylic acid were well binders of metal ions [36]. Shao et al. [37] and Xie et al. [16] found that aspartic acid with carboxyl were attributed to specific binding of (111) Au crystal face, benefitting the growth of (100) set and anisotropic growth of Au nanoscales. Glutamic acid with carboxyl cover 22.6% in IPE, other large ratio of amino acids (9.14% leucine, 8.37% alanine, and 8.12% glycine) did not contribute to the binding of nanoparticles. Besides, cysteine was an excellent gold binder, possessing a sulfhydryl (SH) functional group that can assist to modify metal surfaces [38, 39]. Balasubramanian et al. [40] analyzed the gold nanoscales by energy dispersive X-ray analysis (EDAX), finding that sulfur existed in the tail of the nanoscale rather than in its middle. It indicates that sulfur in amino acids were shape director. IPE contained 1.17% cysteine, but it did not exist in component of 10–30 kDa and there was no significant difference in the ratio of methionine between IPE and 10–30 kDa ($P=0.250>0.05$), which also own sulfur element. As the analysis above, IPE was not good at controling the morphology of AuNPs.

The synthesis processes of AuNPs could be summarized that gold ions were first adsorbed through amino acids like lysine and their functional groups by electrostatic attraction, and later Au was reduced from Au (III) to Au (I) and then to Au (0). The growth of AuNPs occurred through the initial nucleation step, followed by depositional growth and oriented adhersion with the help of different amino acids like glutamic

acid and methionine. AuNPs with monodisperse size and morphology were obtained and stabilized with the capping of protein molecules (Figure 8).

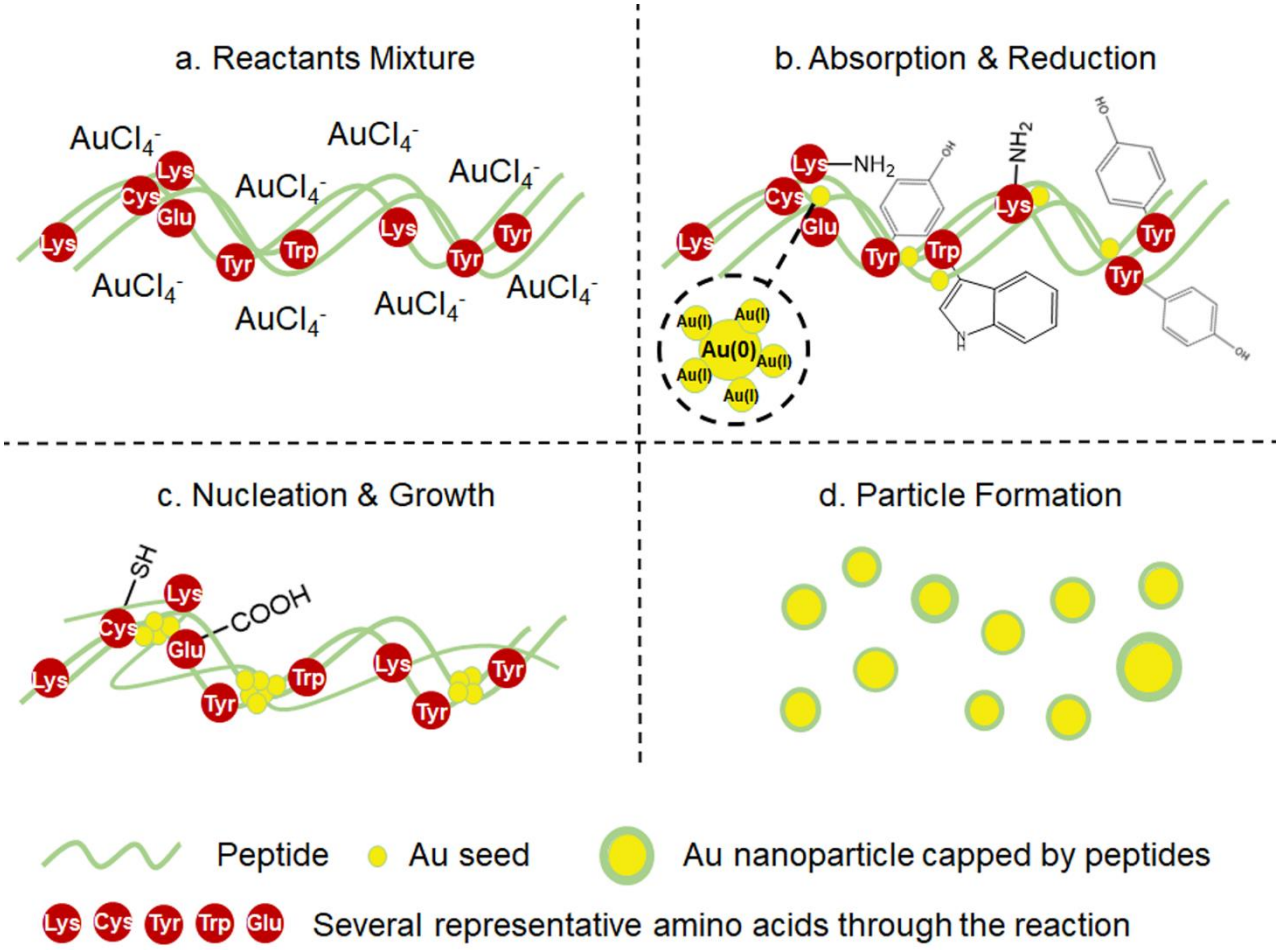

Figure 8: Simulated synthesis processes of gold nanoparticles.

Conclusion

A simple synthesis based on the bioreduction ability of *P. sanguineus* extract solution has been developed to produce spherical AuNPs. The IPE of *P. sanguineus* could be successfully graded into five fractions by ultrafiltration approach which was used to synthesize AuNPs, respectively. Comparing with the original IPE and other fractions, 10–30 kDa fraction obtained AuNPs with the most concentrated size smaller than 30 nm in high yield (above 90%) and the most homogeneous shape (87% spherical

shapes). Under the optimized conditions of 25 ml 10–30 kDa fraction, pH=4, 30 ℃ and 0.5 mM $AuCl_4^-$,the recovery of AuNPs could achieved to 94.64%, and 93.5% of AuNPs were spherical shapes, with the size range from 6 nm to 25 nm. FTIR and XPS revealed that carbonyl, hydroxyl, amine, and carboxyl might be involved in the recovery process. The mechanism might be mainly contributed by the reduction and formation of AuNPs with smaller size by larger proportion of lysine and tyrosine, and the generation of spherical products with low content of amino acids for anisotropic growth such as cysteine. More study on purified protein of 10–30 kDa fraction will be carried out to synthesize controllable AuNPs rapidly and efficiently. The work provided the basis for improving the performance of AuNPs and gave the ease of peptide sequence design for the synthesis of nanomaterials.

Experimental

Materials and reagents

Chloroauric acid ($HAuCl_4 \cdot 3H_2O$), dextrose, KH_2PO_4, $MgSO_4 \cdot 7H_2O$ and other chemicals were purchased from Aladdin, Shanghai, China. Chloroauric acid was dissolved in ultrapure water to prepare stock solution for further use. Ultrafiltration tube (Amicon Ultra-15, Millipore) was obtained from Millipore Inc. pH were adjusted using NaOH or HCl and all reagents were of analytical grade.

Instruments and analytical methods

The remaining gold ion concentration was determined by flame atomic absorption spectroscopy (FAAS) (Shimadzu, A680, Japan) and the absorbance was measured by UV-vis spectrophotometer (Shimadzu, UV-2450, Japan). The quantitation of total

protein from P2 was tested using Pierce™ Rapid Gold BCA Protein Assay Kit (Thermo Fisher Scientific, China). The elemental analysis of nanoparticles was examined under vacuum combined with X-ray diffractograms (XRD) using Bruker D8 ADVANCE (Germany) (λ= 0.154 nm). Transmission electron microscope (TEM) images were obtained with JEM-2100 TEM (JEOL, Tokyo, Japan). The data of Fourier transform infrared (FT-IR) spectra (4000–500 cm^{-1}) were collected by Thermo Scientific Nicolet iS10 (Thermo, America) with KBr pellets (Nicolet, America). X-ray photoelectron spectroscopy (XPS) was obtained on a JEOL JAMP-9500F instrument (JEOL, Japan).

Preparation of different fractions of IPE

The fungal strain *P. sanguineus* (CGMCC 5.00815) was grown in the 250 ml potato medium containing dextrose, KH_2PO_4, $MgSO_4 \cdot 7H_2O$ and vitamin at 165 rpm, pH 6 and 30 ℃ for 72 h. Then, the culture was subjected to centrifuge at 10,000 rpm and 4 ℃ for 20 min. The collected biomass was washed five times with ultrapure water and was resuspended in 24 ml sterile ultrapure water. The resuspended biomass was sonicated by ultrasonic cell disruptor (VCX150, SONICS, America) for 10 min at 60% amplitude to prepare IPE [13]. The cell debris was removed by centrifugation, and the supernatant was diluted to 24 ml again (denoted as IPE).

IPE was ultrafiltrated (ultrafiltration tube, Amicon Ultra-15, Millipore) to obtain proteins, which owned filter device to gain corresponding interception of proteins by centrifugal force (5000 rpm, 15 min and 4 ℃). After centrifugation, the liquid below the ultrafiltration tube was put into another filter device which could intercept smaller protein, so the quality interval products of IPE could be obtained. Briefly, IPE could

be separated into five fractions: the molecular-weight (MW) of <10 kDa (P1), 10–30 kDa (P2), 30–50 kDa (P3), 50–100 kDa (P4) and >100 kDa (P5). IPE and five fractions were then determined by SDS-PAGE analysis.

Biosynthesis of AuNPs

In order to identify the effect of AuNPs, the above mentioned five fractions of P1–P5 and IPE were mixed with $HAuCl_4$ solution separately and the mixture was reacted at 0.5 mM final gold ion concentration, pH 4, 165 rpm, and 30 ℃ for 24 h after being diluted to 50 ml final volume. The remaining gold ion concentration and the formed AuNPs were analyzed. The optimal fraction of IPE was judged by recovery efficiency of gold ions, morphology and size distribution of AuNPs.

To obtain the optimum conditions of synthesis of AuNPs by the selected fraction (P2) of IPE, the effects of P2 dosage (10, 15, 20 and 25 ml, protein concentration of 0.87 mg/ml), final gold ion concentration (0.1, 0.3, 0.5, 0.7 and 1.0 mM) and pH value (2, 4, 6, 8, 10 and 12) were studied. All experiments were conducted in triplicates.

Characterization of AuNPs synthesized by P2 at optimum condition

AuNPs were collected by centrifuging at 11,000 rpm for 10 min, purified by ultrapure water repeatedly for three times and then freeze-dried. The crystalline properties of AuNPs were confirmed by XRD. The chemical properties of 10–30 kDa fraction, the surface and synthesis mechanism of AuNPs were analyzed by FT-IR and XPS.

Amino acid analysis of IPE and 10–30 kDa fraction

The level of amino acids were analyzed by membraPure Amino acid analyzer (A300, Germany). Fresh samples of IPE and 10–30 kDa were pretreated by alkali (LiOH)

hydrolysis. The standard and test sampling concentration are controlled around 100 nmol/ml and the processes are automatic injection (Sample volume: 20 μL), gradient elution (flow velocity: 160 μL/min, ninhydrin post-column derivatization (flow velocity: 80 μL/min) and detection of dual channel visible photometer (570 nm and 440 nm). The chromatographic column is membraPure T259 sodium ion-exchange column. Typical chromatogram of amino acids standard solution are shown in Supporting Information File 1, Figure S7 and S8.

Statistical analysis

The data were analyzed using the mean and standard deviation was calculated and expressed as error bars. Further statistical analysis was performed using SPSS 17.0.0 (SPSS Inc., 2008) and the independent sample t-test was performed to examine the statistical difference of the gold recovery capacities between IPE and five fractions of IPE, and the level of amino acids between IPE and P2.

Supporting Information

Supporting Information File 1:

File Name: Additional experimental details

File Format: Word

Title: Supporting Materials

Acknowledgements

This work was financially supported by the Guangdong Science and Technology Project (2017A020216013), the Fundamental Research Funds for the Central

Universities (2017PY012) and the Guangzhou Science and Technology Project (201604020055).

References

1. Du, J. J.; Du, H.; Ge, H. Y.; Fan, J. L.; Peng, X. J. *Sensors and Actuators B: Chemical,* **2018,** *255,* 808–813.
2. Fang, X. N.; Zheng, Y. Z.; Duan, Y. K.; Liu, Y.; Zhong, W. W. *Analytical Chemistry*, **2018**, *91*, 482–504.
3. Huang, J. L.; Lin, L. Q.; Sun, D. H.; Chen, H. M.; Yang, D. P.; Li, Q. B. *Chemical Society Reviews*, **2015**, *44*, 6330–6374.
4. Kumar, S.; Kumar, A.; Kim, G. H.; Rhim, W. K.; Hartman, K. L.; Nam, J. M. *Small*. **2017**, *13*, No. 1701584.
5. Sheng, J. P.; Wang, L. Q.; Han, Y. J.; Chen, W. S.; Liu, H.; Zhang, M; Deng, L.; Liu, Y. N. *Small*, **2018**, *14*, No. 1702529.
6. Kang, N. X.; Zhu, N. W.; Guo, W. Y.; Shi, C. H.; Wu, P. X.; Wei, X. R. *Chemical Engineering Journal*, **2018**, *334*, 99–107.
7. Shi, G. R.; Li, Y. L.; Xi, G. H.; Xu, Q. Q.; He, Z. J.; Liu, Y. T.; Zhang, J. H.; Cai, J. *Journal of Hazardous Materials.* **2017**, *335*, 170–177.
8. Tang, Y. N.; Sun, H.; Shang, Y. X.; Zeng, S.; Qin, Z.; Yin, S. Y.; Li, J. Y.; Liang, S.; Lu, G. L.; Liu, Z. N. *Journal of Colloid and Interface Science*, **2019**, *535*, 516–523.
9. Kariuki, V. M.; Hoffmeier, J. C.; Yazgan, I.; Sadik, O. A. *Nanoscale*, **2017**, *9*, 8330–8340.
10. Vaseghi, Z.; Nematollahzadeh, A.; Tavakoli, O. *Review in Chemical Engineering*, **2018**, *34*, 529–559.

11. Dahoumane, S. A.; Mechouet, M.; Wijesekera, K.; Filipe, C. D. M.; Sicard, C.; Bazylinski, D. A.; Jeffryes, C. *Green Chemistry*, **2017**, *19*, 552–587.
12. Faramarzi, M. A.; Forootanfar, H. *Colloids and Surfaces B: Biointerfaces*, **2011**, *87*, 23–27.
13. Shi, C. H.; Zhu, N. W.; Cao, Y. L.; Wu, P. X. *Nanoscale Research Letters*, **2015**, *10*, No. 147.
14. Shen, W. L.; Qu, Y. Y.; Li, X. Y.; Pei, X. F.; You, S. N.; Yin, Q. X.; Wang, J. W.; Ma, Q. *Environmental Science and Pollution Research*, **2018**, *25*, 13626–13632.
15. Italiano, F.; Agostiano, A.; Belviso, B. D.; Caliandro, R.; Carrozzini, B.; Comparelli, R.; Melillo, M. T.; Mesto, E.; Tempesta, G.; Trotta, M. *Colloids and Surfaces B: Biointerfaces*, **2018***, 172*, 362–371.
16. Xie, J. P.; Lee, J. Y.; Wang, D. I. C.; Ting, Y. P. *Small*, **2007**, *3*, 672–682.
17. Chang, W. S.; Willingham, B.; Slaughter, L. S.; Dominguez-Medina, S.; Swanglap, P.; Link, S. *Accounts of Chemical Research*, **2012**, *45*, 1936–1945.
18. Rogers, N. J.; Claire, S.; Harris, R. M.; Farabi, S.; Zikeli, G.; Styles, I. B.; Hodges, N. J.; Pikramenou, Z. *Chemical Communication*, **2014**, *50*, 617–619.
19. Narayanan, K.B.; Sakthivel, N. *Advances in Colloid and Interface Science*, **2010**, *156*, 1–13.
20. Guo, R.; Jiao, T. F.; Xing, R. R.; Chen, Y.; Guo, W. C.; Zhou, J. X.; Zhang, L. X.; Peng, Q. M. *Nanomaterials*, **2017**, *7*, No. 10.
21. Das, S. K.; Das, A. R.; Guha, A. K. *Small*, **2010**, *6*, 1012–1021.
22. Zhu, N. W.; Cao, Y. L.; Shi, C. H.; Wu, P. X.; Ma, H. Q. *Environmental Science and Pollution Research*, **2016**, *23*, 7627–7638.
23. Velamakanni, A.; Magnuson, C. W.; Ganesh, K. J.; Zhu, Y.; An, J.; Ferreira, P. J.; Ruoff, R. S. *Acs Nano*, **2010**, *4*, 540–546.

24. Choudhary, B. C.; Paul, D.; Gupta, T.; Tetgure, S. R.; Garole, V. J.; Borse, A. U.; Garole, D. J. *Journal of Environmental Sciences*, **2017**, *55*, 236–246.
25. Gonzalez, E.; Arbiol, J.; Puntes, V. F.; *Science*, **2011**, *334*, 1377–1380.
26. Kang, F.; Qu, X.; Alvarez, P. J. J.; Zhu, D. *Environmental Science and Technology*, **2017**, *51*, 2776–2785.
27. Kanchi, S.; Kumar, G.; Lo, A. Y.; Tseng, C. M.; Chen, S. K.; Lin, C. Y.; Chin, T. S. *Arabian Journal of Chemistry*, **2018**, *11*, 247–255.
28. Philip, D. *Spectrochimica Acta Part A: Molecular and Biomolecular Spectroscopy*, **2009**, *73*, 374–381.
29. Corra, S.; Shoshan, M. S.; Wennemers, H. *Current Opinion in Chemical Biology*, **2017**, *40*, 138–144.
30. Gurunathan, S.; Han, J.; Park, J. H.; Kim, J. H. *Nanoscale Research Letters*, **2014**, *9*, No. 248.
31. Das, S. K.; Liang, J.; Schmidt, M.; Laffir, F; Marsili, E. *Acs Nano*, **2012**, *6*, 6165–6173.
32. Tan, Y. N.; Lee, J. Y.; Wang, D. I. C. *Journal of the American Chemical Society*, **2010**, *132*, 5677–5686.
33. Munro, C. J.; Hughes, Z. E.; Walsh, T. R.; Knecht, M. R.; *Journal of Physical Chemistry C*, **2016**, *120*, 18917–18924.
34. Bhargava, S. K. Booth, J. M.; Agrawal, S.; Coloe, P.; Kar, G. *Langmuir*, **2005**, *21*, 5949-5956.
35. Nguyen, M. A.; Hughes, Z. E.; Liu, Y.; Li, Y.; Swihart, M. T.; Knecht, M. R.; Walsh, T. R. *Journal of Physical Chemistry C*, **2018**, *122*, 11532–11542.
36. Corra, S.; Lewandowska, U.; Benetti, E. M.; Wennemers, H. *Angewandte Chemie*, **2016**, *128*, 8542–8545.

37. Shao, Y.; Jin, Y. D.; Dong, S. J. *Chemical Communication*, **2004**, No. 9, 1104–1105.
38. Duan, H. H.; Wang, D. S.; Li, Y. D. *Chemical Society Reviews*, **2015**, *44*, 5778–5792.
39. Monti, S.; Barcaro, G.; Sementa, L.; Carravetta, V.; Agren, H. *Nano Research*, **2018**, *11*, 1757–1767.
40. Balasubramanian, S.; Bezawada, S. R.; Raghavachari, D. *Acs Sustainable Chemistry and Engineering*, **2016**, *4*, 3830–3839.